NACA RM L56A16

NACA

RESEARCH MEMORANDUM

FLIGHT INVESTIGATION OF THE EFFECT OF A PROPULSIVE JET POSITIONED ACCORDING TO THE TRANSONIC AREA RULE ON THE DRAG COEFFICIENTS OF A SINGLE-ENGINE DELTA-WING CONFIGURATION AT MACH NUMBERS FROM 0.83 TO 1.36

By Joseph H. Judd and Ralph A. Falanga

Langley Aeronautical Laboratory
Langley Field, Va.

NATIONAL ADVISORY COMMITTEE
FOR AERONAUTICS

WASHINGTON

April 13, 1956
Declassified May 29, 1959

NACA RM L56A16

NATIONAL ADVISORY COMMITTEE FOR AERONAUTICS

RESEARCH MEMORANDUM

FLIGHT INVESTIGATION OF THE EFFECT OF A PROPULSIVE JET POSITIONED ACCORDING TO THE TRANSONIC AREA RULE ON THE DRAG COEFFICIENTS OF A SINGLE-ENGINE DELTA-WING CONFIGURATION AT MACH NUMBERS FROM 0.83 TO 1.36

By Joseph H. Judd and Ralph A. Falanga

SUMMARY

A 60° delta-wing configuration with an engine location in a pod contiguous to the underside of the fuselage was flight tested to determine the effects of the flow field of and about the propulsive jet on the drag, lift, and longitudinal stability. A solid-propellant rocket motor was used to simulate the sonic exhaust jet of a turbojet engine plus afterburner and operated at a jet-exit static-pressure ratio of approximately 4. The jet-on Mach number varied from 0.83 to 1.36 and Reynolds numbers varied from 6.9×10^6 to 10.4×10^6, whereas the jet-off flight covered a Mach number range from 0.83 to 1.63 and Reynolds numbers from 6.9×10^6 to 17.3×10^6.

Jet-on drag coefficients were lower than jet-off drag coefficients at transonic speeds. The maximum difference in drag coefficient, 0.0156, was attained at a Mach number of 0.99. The difference between jet-on and jet-off drag-rise coefficients to a Mach number of 1.0 can be predicted approximately for this configuration by use of the transonic area rule and inclusion of the jet in the cross-sectional-area distribution for the jet-on case. Above a Mach number of 1.27, the jet-off drag coefficients were lower than jet-on drag coefficients for this configuration.

Lift-coefficient increments of 0.045 between jet-on and jet-off flight were attained to a Mach number of 0.92.

INTRODUCTION

Recent investigations of the effect of the propulsive jet on the aerodynamic characteristics of bodies and airplane configurations have shown that important changes in drag and lift coefficients can occur between jet-on and jet-off conditions. For example, positive increments in base and boattail pressure coefficients, caused by the jet expansion, have reduced drag coefficients between jet-on and jet-off conditions for bodies of revolution with jet exhausting from the base (refs. 1 and 2). Also, the flow field produced by the expansion of the jet, when located in a favorable position below the wing, has been shown in references 3, 4, and 5 to produce appreciable increments in lift from the jet-off conditions. It was proposed, therefore, to use the expansion of the jet to reduce the drag from the jet-off condition of an airplane configuration by the application of the concept of the transonic area rule (ref. 6) for the jet-on condition. In this case the jet was considered a solid body and was used to fill the cross-sectional-area distribution and reduce its slope at the rear of the configuration. A model of a 60° delta-wing interceptor configuration, whose single engine was located in a pod contiguous to the underside of the fuselage and designed according to the above-stated principle, was flight tested by the Pilotless Aircraft Research Division of the Langley Aeronautical Laboratory as part of a current program on jet effects.

The jet exit was located slightly ahead of the wing trailing edge and below the wing. The propulsive jet issuing from the sonic exhaust nozzle simulated exhaust parameters of a current turbojet plus afterburner at an altitude of 35,000 feet and a Mach number of 1.3 by utilizing a solid-propellant rocket motor designed according to reference 7.

The flight test was made at the Langley Pilotless Aircraft Research Station at Wallops Island, Va. The Mach number range of this test was from 0.83 to 1.63 for jet-off flight and 0.83 to 1.36 for jet-on flight. The jet-off Reynolds number range varied from 6.9×10^6 to 17.3×10^6 and jet-on Reynolds number range from 6.9×10^6 to 10.4×10^6.

SYMBOLS

ac	distance from leading edge of mean aerodynamic chord to aerodynamic center, percent mean aerodynamic chord, positive rearward
A	cross-sectional area, sq ft

b wing span, ft

c wing chord, ft

$\bar{c}$ wing mean aerodynamic chord, ft

$C_{p,B}$ base pressure coefficient, $\frac{p_B - p_\infty}{q}$

C_D drag coefficient, $\frac{\text{Drag}}{qS}$

C_L lift coefficient, $\frac{\text{Lift}}{qS}$

C_{L_α} lift-curve slope, $\frac{dC_L}{d\alpha}$ per deg

$C_{L,T}$ trim-lift coefficient

C_m pitching-moment coefficient, measured about model center of gravity

$C_{m,j}$ pitching moment due to jet thrust about center of gravity

C_{m_α} static-stability derivative, $\frac{dC_m}{d\alpha}$ per degree

$C_{m_q} = \frac{\partial C_M}{\partial\left(\frac{\dot{\theta}\bar{c}}{2V}\right)}$ per radian

$C_{m_{\dot{\alpha}}} = \frac{\partial C_M}{\partial\left(\frac{\dot{\alpha}\bar{c}}{2V}\right)}$ per radian

$\left(C_{m_q} + C_{m_{\dot{\alpha}}}\right)$ longitudinal damping derivatives, per radian

I_y moment of inertia in pitch about model center of gravity, slug-ft^2

l fuselage length, ft

M Mach number

p_B engine-pod base pressure, lb/sq ft

p_e jet-exit static pressure, lb/sq ft

p_∞ free-stream static pressure, lb/sq ft

P period of short-period longitudinal oscillation, sec

q dynamic pressure, lb/sq ft

r radius of equivalent body, ft

R Reynolds number, based on wing mean aerodynamic chord

S total plan form area, sq ft

t time from launch, sec

$t_{1/2}$ time required for short-period oscillation to damp to one-half amplitude, sec

t/c wing-thickness ratio

V velocity, ft/sec

W weight of model, lb

x distance along fuselage measured from nose of engine pod, ft

x_1 distance of center of gravity from leading edge of wing mean aerodynamic chord, positive rearward

z distance of center of gravity from leading edge of wing mean aerodynamic chord, positive upward

α angle of attack at the center of gravity, measured from fuselage center line, deg

α_T trim angle of attack, deg

$\dot{\alpha} = \frac{1}{57.3} d\alpha/dt$, radians/sec

θ angle of pitch at the model center of gravity, measured from fuselage center line, radians

$\dot{\theta} = \frac{d\theta}{dt}$, radians/sec

MODEL AND APPARATUS

Model

A three-view drawing of the flight model is shown in figure 1 and the basic geometric parameters are given in table I. The present model was derived from a research configuration (model 7 of ref. 8) which had a 60° delta wing mounted on a parabolic body of revolution and no horizontal tail. The test configuration utilized an engine installation located in a pod contiguous to the underside of the fuselage. To ensure dynamic lateral stability in the test model two auxiliary fins were mounted at the rear of the engine pod. The use of two fins was dictated by the underslung booster configuration.

The basic fuselage was a parabolic body of revolution. To house the propulsive unit an engine pod was mounted on the underside of the fuselage, 4.3 inches below the fuselage center line. To cope with the problems of telemeter installation, a nose fairing and a cylindrical section were mounted ahead of the engine pod. Ordinates of the fuselage and pod are given in table II. A conical boattail of 3.92° half-angle was used on the engine pod. Figure 2, a drawing of the engine, shows the rear of the pod and the jet and base diameters.

The wing used on the configuration was a 60° delta wing of solid magnesium whose thickness ratio varied from 3 percent at the root to 6 percent at the tip. The airfoil had a flat center section, 0.5c, which was located rearward of 0.3c. Leading and trailing edges were faired to the flat center section by using NACA airfoils as shown in figure 3. The vertical fin was swept 60° at the leading edge and had a hexagonal airfoil section whose thickness ratio varied from 1.7 percent at the root to 3.2 percent at the tip. Two auxiliary fins at a 45° angle below the wing plane were attached to the engine pod. These fins were flat steel plates, 0.125 inch thick, with sharpened leading and trailing edges.

The basic turbojet simulator utilized in this model consisted of a combustion chamber, a flow control nozzle, and a convergent sonic-exit nozzle. A Cordite SU/K propellant grain 23.6 inches long generated the exhaust gases to simulate a current turbojet plus afterburner (ref. 7). The jet-exit diameter was 3.792 inches and the jet base diameter was 4.125 inches, corresponding to a jet area of 0.0786 square foot and a base area of 0.0925 square foot. Figure 4 shows the relationship of the jet exhaust nozzle, the fuselage, fins, and wing.

Booster and Equipment

An underslung booster, as shown in figure 5 and described in reference 9, was used to propel the model to maximum velocity. Two lugs, shown in figure 2, were welded to the engine pod in order to provide a forward attachment between the model and booster. The rear booster attachment was provided with an adapter which fitted in the exhaust nozzle of the model.

Instrumentation

A six-channel telemeter, located in the nose of the engine pod, continuously transmitted measurements of free-stream total pressure, angle of attack, longitudinal and normal acceleration, combustion chamber static pressure, and nozzle static pressure. The locations of the pressure orifices used to measure combustion chamber static pressure and the exit-nozzle static pressure are shown in figure 2. The longitudinal accelerometer was located at station 54.747 and in the wing mean chord plane, whereas the normal accelerometer was located at station 52.625 and in the wing mean chord plane. Data for the flight tests were obtained by use of telemeter, CW Doppler velocimeter, NACA modified SCR 584 tracking radar and rawinsonde. Model velocity, obtained with the velocimeter, was corrected for wind velocity which was determined from rawin measurements.

TEST PROCEDURE

Tests

The turbojet simulator combustion chamber pressure, nozzle static pressure, and thrust were measured in a preflight motor firing in the Langley rocket test area. Using these data, calibration curves of the rocket thrust as a function of both the combustion chamber pressure and the nozzle static pressure were obtained. The purpose of measuring thrust by two independent instruments was to provide insurance against the malfunctioning of a pressure cell during the flight.

The flight model was launched from a mobile launcher (fig. 5). An underslung, single ABL Deacon rocket motor boosted the configuration to the peak Mach number. Jet-off data were obtained during the decelerating flight after separation of model from the booster. Jet-on data were obtained during firing of the turbojet simulator which was started at the lowest test Mach number in the deceleration phase. During jet-off flight the model was disturbed in pitch by separation from the booster,

and later by a pulse rocket. During jet-on flight the model was disturbed in pitch when the turbojet simulator was started and when the model passed a Mach number of 1.0. A time history of the angle of attack during the flight is given in figure 6. From an examination of this figure, it can be seen that the angle-of-attack disturbance caused by separation of the model from the booster has been modulated and, from past experience, indicates that a lateral disturbance probably occurred at the same time. Since the model was not instrumented for lateral disturbances, the pitching data obtained during this portion of the flight cannot be analyzed. Also marked on this figure is the time when the second pulse rocket fired, at which time several instruments failed. These were the longitudinal and normal accelerometers and the combustion chamber static pressure. Since the angle of attack was corrected to the model center of gravity during pitching disturbances by using data from the accelerometers, the values of angle of attack shown in figure 6 were stopped at the time when the accelerometers failed. Data beyond this point were obtained after the pulse rocket disturbance damped but were not plotted in figure 6.

The variation of Reynolds number (based on wing mean aerodynamic chord) with Mach number for jet-on and jet-off flight is presented in figure 7. Time histories of velocity, Mach number, and free-stream dynamic pressure during the flight are given in figures 8 and 9.

Analysis

Longitudinal accelerations of the model were obtained from two sources: (1) longitudinal accelerometer and (2) differentiation of the model velocity. Thus, when the longitudinal accelerometer failed, drag was still obtainable. The method of obtaining jet-on and jet-off drag coefficients is explained in reference 1.

The angle-of-attack indicator was mounted ahead of the nose and the measured angles of attack were corrected to those at the model center of gravity, according to reference 10.

The method of obtaining lift and longitudinal stability coefficients from transient longitudinal disturbances is given in reference 11. During jet-on flight, the model weight, moment of inertia, and center of gravity changed as the rocket fuel burned. The variation of these quantities with time is given in figures 10 and 11. All data obtained during pitching oscillations were computed using these values.

The engine-pod base pressure coefficient was computed from the exit-nozzle static pressure during jet-off flight. It was assumed that the exit-nozzle static pressure represented the magnitude of base pressure occurring over the entire base.

ACCURACY

To establish telemeter instrument accuracies, statistical data have been compiled on flight instrument measurements over a number of years, and on the basis of this information the maximum probable error is believed to be 1 percent of the full-scale calibrated range for the telemetered measurements. These maximum probable errors in measurements, which have been used to compute the errors in base pressure, drag, and lift coefficients for several Mach numbers, are tabulated below.

Mach number	C_{P_b}	$C_{D_{jet\text{-}off}}$	$C_{D_{jet\text{-}on}}$	$C_{L_{jet\text{-}off}}$
0.95	±0.097	±0.0067	±0.0092	±0.0176
1.25	±.052	±.0036	±.0054	±.0047
1.60	±.028	±.0021	-------	±.0023

The velocity measured by the CW Doppler velocimeter is known to have an error of less than 1 percent at supersonic speeds and less than 2 percent at subsonic speeds. Since Mach number is determined from velocity, the above-quoted errors also apply to Mach number.

The magnitude of these computed errors is large in comparison with the magnitude of the measured coefficients. However, the longitudinal accelerations used to compute the chord force coefficients were measured directly by telemeter and also were obtained by differentiation of the model velocity. These values were compared and were nearly the same, the difference being much smaller than the stated error. The measured motor pressures were compared with those obtained from the static test firing and the specific impulses of the two firings were compared. These also were much closer than the quoted accuracies. Because of these checks it is believed that the error of the jet-on drag coefficients is no more than ±0.003, which is equal to the scatter of the data obtained during pitching oscillations. Similarly, the error in jet-off drag coefficients is approximately ±0.002.

RESULTS AND DISCUSSION

Drag

The variation of total drag coefficient with angle of attack, obtained during pitching disturbances, is given in figure 12. Since jet-off drag coefficients were obtained during pitching oscillations at

supersonic speeds, and jet-on drag coefficients were obtained during pitching oscillations at transonic and sonic speeds, a direct comparison of these data cannot be made. Although the jet-off drag coefficients show hysteresis as the model pitches, the minimum drag coefficient apparently occurs at 0° angle of attack and for the small angle-of-attack range covered exhibits little variation with angle of attack. The jet-on drag coefficients show the same effect. Thus, when a comparison between trim drag coefficients for jet-on and jet-off flight is made, the effect of the difference in trim angle of attack will be neglected inasmuch as the maximum trim angles were less than $\pm 1^\circ$.

The variation of jet-on and jet-off total drag coefficients is presented in figure 13, together with the base drag coefficient of the engine pod. The trim angle of attack for jet-on and jet-off flight is plotted in figure 14 and values of the jet-exit static-pressure ratio in figure 15. During the period of jet-on flight, the jet-exit static-pressure ratio is approximately 4.0 and remains relatively constant, corresponding to flight with a current turbojet-plus-afterburner at 35,000 feet altitude and a Mach number of 1.3.

The total jet-on drag coefficients are lower than the total jet-off drag coefficients to a Mach number of 1.26 and reach a maximum difference of 0.0156 at $M = 0.99$. Above a Mach number of 1.26, the jet-off drag coefficients are less than the jet-on drag coefficients. By subtracting the base drag coefficient from the jet-off drag coefficient, the effect of the jet on the external drag can be determined. The difference between total jet-off drag coefficients (less base drag coefficients) and jet-on drag coefficients is plotted in figure 16. It should be noted that the maximum reduction in drag coefficient occurs approximately at Mach number 1.0. As was mentioned in the introductory remarks, the jet was located to fill out the cross-sectional-area distribution. Naturally, after Mach number 1.0 the Mach lines from the jet sweep back at greater angles. The influence of the jet is thus caused to affect a much smaller part of the configuration and thereby to lower drag coefficient differences between jet-on and jet-off operation.

The variation of model cross-sectional area along the longitudinal axis of the configuration and its equivalent body of revolution is given in figure 17. On the side view of the configuration are several curves showing the jet shape for different flight conditions. The jet bulge was measured from schlieren photographs of a sonic jet operating in the 8-foot transonic wind tunnel at a Mach number of 1.0, and shadowgraph pictures of a sonic jet operating at a Mach number of 1.4 in the preflight jet of the Langley Pilotless Aircraft Research Station at Wallops Island, Va. The measured values of jet diameter are close in magnitude. The value of jet cross-sectional area at a Mach number of 1.0 was used and a cylindrical jet shape was assumed after the initial bulge. The peak drag-rise coefficient

was computed for the jet-on and jet-off case using the curves of reference 13. The jet-off peak drag rise was 0.020 which agrees with the measured peak drag rise of the configuration. The computed jet-on peak drag-rise coefficient was 0.0076. This should be expected to apply only at or slightly above a Mach number of 1.0. The subsonic level of the jet-on drag coefficients was taken as the value at a Mach number of 0.85. Using this value, the drag rise to a Mach number of 1.02 (which was the same as the Mach number for jet-off peak drag rise) was 0.0119. Thus while the value of drag rise to sonic speeds was higher than the estimated value for jet-on flight, the transonic area rule does predict a pressure drag reduction between jet-off and jet-on flight.

Above a Mach number of 1.27 the jet-on drag coefficients are greater than the jet-off total drag coefficients. Thus the approach used to reduce the drag coefficients applied only for the Mach number range for which it was intended.

The total drag coefficient for jet-off flight appeared to be high, as seen in figure 13. In order to check on these values, an attempt was made to estimate the drag coefficients of the configuration by addition of the drag coefficients of the components. Drag coefficients for the wing, body, and vertical tail were obtained from reference 8; boattail drag coefficients for the engine pod were obtained from reference 13 and skin-friction drag coefficients from reference 14. The auxiliary fins were assumed to be flat plates and have turbulent skin friction over the surface. Drag coefficients for these fins were estimated from reference 14. These values are plotted in figure 18 and a considerable difference is shown to exist between the measured and estimated total drag coefficients with the estimated values being 0.0043 to 0.0068 below the measured drag coefficients. Since the estimated values of pressure drag rise agree with the measured drag rise, the difference in drag level is attributed to drag caused by the interference of engine pod and fuselage. A similar drag difference caused by an unfavorable wing-fuselage juncture was observed in reference 15; and also, the high drag level of model 2 of reference 9 was attributed to a similar fuselage-engine pod juncture.

Values of engine-pod base-drag coefficient presented in figure 13 were obtained from a pressure measured at the wall inside the convergent sonic nozzle. Pressure coefficients for this orifice are presented in figure 19. These coefficients are considerably higher than values for a cylindrical conical afterbody (ref. 14) with approximately the same boattail angle.

Lift

The variations of lift coefficient with angle of attack obtained during pitching oscillations for jet-on and jet-off flight are given in

figure 20. Flagged symbols indicate increasing values of angle of attack, while unflagged symbols indicate decreasing angles of attack. Since the jet-on and jet-off lift coefficients were not obtained at the same Mach numbers, a direct comparison cannot be made. However, the jet-on data, as shown in figure 20a, indicate that at $\alpha = 0$ the jet gives positive increments in lift coefficients, but that these decrease with increasing Mach number. It is felt that this variation of incremental lift coefficient at $\alpha = 0$ with Mach number is a result of the disturbance caused by the jet moving rearward of the wing as free-stream Mach number is increased. Thus, it appears that the operation of the jet increased the model lift in the transonic speed range of the present test in a manner comparable to that reported at supersonic speeds in reference 5.

Although the angle-of-attack range was limited, it appeared that during the transonic speeds of the jet-on flight the lift curve was S-shaped. Thus, at some subsonic Mach numbers two values of lift-curve slope were obtained: (1) a value for $\alpha = 0$, and (2) a value for a greater angle of attack. The variation of the slope of the lift curve C_{L_α} with Mach number for jet-on and jet-off flight is presented in figure 21 together with variation of lift-curve slope for a 60° delta-wing—body combination (ref. 17). The jet-on and jet-off data presented are in agreement with reference 17, except at the lower Mach numbers. In this speed range the lift curve had a tendency to be S-shaped which resulted in lower values of lift-curve slope near $\alpha = 0$ hence, the cause for disagreement with reference 17 at the lower Mach numbers.

Trim

The variation of trim angle of attack with Mach number is presented in figure 14 for jet-on and jet-off flight. During jet-off flight, the configuration trims at positive angles of attack from transonic speeds to Mach number 1.24, whereas during jet-on flight, the configuration trims at a negative angle of attack at Mach numbers below 1.00. From these data, it can be seen that the greatest change in trim angle of attack between jet-on and jet-off flight occurs below $M = 0.92$ and that the jet-on trim angle of attack is nearly 1.5° below the jet-off trim angle of attack. The effect of the jet is large at Mach numbers from 0.83 to 0.92; this effect causes the model to trim negatively even though the turbojet simulator thrust was tending to trim it positively. It is felt that the radical trim change which occurred during jet-on flight was caused by the rearward shift of the jet effect on the wing and afterbody of the model as the Mach number increased. The trim-lift coefficient $C_{L,T}$ for jet-on and jet-off flight is given in figure 22. The plot indicates positive $C_{L,T}$ for both jet-on and jet-off flight of approximately the same order of magnitude. This indicates that the flow field of the jet produces an appreciable lift-coefficient increment

in this speed range as great as 0.045 at a Mach number of 0.85 and also, as mentioned above, an appreciable nose-down pitching moment. The thrust of the jet produces a nose-up pitching moment whose variation with time is plotted in figure 23. The reduction in magnitude (from 0.026 to 0.0115) of the pitching-moment coefficient due to thrust is mainly due to the increase in dynamic pressure as the speed increases, since the thrust remained relatively constant during jet-on flight.

Longitudinal Stability

The period of the short-period longitudinal oscillations is given in figure 24. The pitching oscillations are a result of disturbing the model in pitch by firing pulse rockets during jet-on and jet-off flight and by firing the turbojet simulator. The static stability for the model is presented in figures 25 and 26, where the variation of the static-stability derivative $\frac{dC_m}{d\alpha}$ and aerodynamic center with Mach number are shown, respectively. The period was used to compute C_{m_α}, and these C_{m_α} and experimental C_{L_α} were employed to compute the aerodynamic center. The general trend of jet-on C_{m_α} with Mach number appears normal for wing-body combinations of this type as does the aerodynamic center. The aerodynamic center moves rearward with increasing Mach number, as expected, but the values of ac presented at $M \cong 1.00$ appear to be somewhat on the high side as compared to what would be expected for the wing-body combination. Probably the auxiliary fins contributed to the increased rearward shift of the ac.

The time required for the short-period longitudinal oscillation to damp to one-half amplitude is shown in figure 27 and the damping derivatives $C_{m_q} + C_{m_{\dot{\alpha}}}$ are shown in figure 28. The damping derivatives indicate that the model is dynamically longitudinally stable throughout the test Mach number range. Also plotted in figure 27 is a theoretical curve of damping derivatives for this model at supersonic speeds, computed by method of reference 18. The supersonic experimental values from this test indicate good agreement with the theoretical values.

CONCLUDING REMARKS

A flight investigation of a 60° delta-wing configuration with an engine location in a pod contiguous to the underside of the fuselage was

made to determine the effect of the propulsive jet on the drag, lift, and longitudinal stability. The jet-exhaust nozzle was located at 91.62 percent of the wing root chord and 1.136 jet diameters below the wing mean chord plane. Jet-on data covered a Mach number range from 0.83 to 1.36 and Reynolds numbers from 6.9×10^6 to 10.4×10^6, whereas jet-off Mach numbers were obtained from 0.83 to 1.63 and Reynolds numbers from 6.9×10^6 to 17.3×10^6. The jet-exit static-pressure ratio was approximately 4.0. The following statements summarize the results:

1. Jet-on drag coefficients were lower than jet-off drag coefficients at transonic speeds. The drag-coefficient difference reached a maximum value at 0.0156 at a Mach number of 0.99. Above a Mach number of 1.26, the jet-off drag coefficients were lower than jet-on drag coefficients.

2. The transonic-area-rule concept can be used to predict jet effects on drag for this type of configuration.

3. Operation of the jet provided increases in lift coefficient of approximately 0.045 at a Mach number of 0.85. The lift-coefficient increments decreased above a Mach number of 0.92 since as Mach number increased the flow field induced on the wing by the jet moved rearward.

4. At Mach numbers between 0.83 and 0.92, the jet flow field induced a nose-down trim angle of attack despite the nose-up moment due to the thrust of the turbojet simulator. The difference between jet-on and jet-off trim angle was 1.50°. After a Mach number of 0.92, the values for jet-on and jet-off trim angle tended to converge.

Langley Aeronautical Laboratory,
National Advisory Committee for Aeronautics,
Langley Field, Va., January 4, 1956.

REFERENCES

1. Falanga, Ralph A.: A Free-Flight Investigation of the Effects of Simulated Sonic Turbojet Exhaust on the Drag of a Boattail Body With Various Jet Sizes From Mach Number 0.87 to 1.50. NACA RM L55F09a, 1955.

2. Henry, Beverly Z., Jr., and Cahn, Maurice S.: Preliminary Results of an Investigation at Transonic Speeds To Determine the Effects of a Heated Propulsive Jet on the Drag Characteristics of a Related Series of Afterbodies. NACA RM L55A24a, 1955.

3. Bressette, Walter E.: Investigation of the Jet Effects on a Flat Surface Downstream of the Exit of a Simulated Turbojet Nacelle at a Free-Stream Mach Number of 2.02. NACA RM L54E05a, 1954.

4. Bressette, Walter E., and Leiss, Abraham: Investigation of Jet Effects on a Flat Surface Downstream of the Exit of a Simulated Turbojet Nacelle at a Free-Stream Mach Number of 1.39. NACA RM L55L13, 1955.

5. Falanga, Ralph A., and Judd, Joseph H.: Free-Flight Investigation of the Effect of Underwing Propulsive Jets on the Lift, Drag, and Longitudinal Stability of a Delta-Wing Configuration at Mach Numbers From 1.23 to 1.62. NACA RM L55I13, 1955.

6. Whitcomb, Richard T.: A Study of the Zero-Lift Drag-Rise Characteristics of Wing-Body Combinations Near the Speed of Sound. NACA RM L52H08, 1952.

7. De Moraes, Carlos A., Hagginbotham, William K., Jr., and Falanga, Ralph A.: Design and Evaluation of a Turbojet Exhaust Simulator, Utilizing a Solid-Propellant Rocket Motor, for Use in Free-Flight Aerodynamic Research Models. NACA RM L54I15, 1954.

8. Sandahl, Carl A., and Stoney, William C.: Effect of Some Section Modifications and Protuberances on the Zero-Lift Drag of Delta Wings at Transonic and Supersonic Speeds. NACA RM L53L24a, 1954.

9. Judd, Joseph H.: A Free-Flight Investigation of the Drag Coefficients of Two Single-Engine Supersonic Interceptor Configurations From Mach Number 0.8 to 1.90 to Determine the Effect of Inlet and Engine Locations. NACA RM L55G05a, 1955.

10. Mitchell, Jesse L., and Peck, Robert F.: An NACA Vane-Type Angle-of-Attack Indicator for Use at Subsonic and Supersonic Speeds. NACA TN 3441, 1955. (Supersedes NACA RM L9F28a.)

11. Gillis, Clarence L., Peck, Robert F., and Vitale, A. James: Preliminary Results From a Free-Flight Investigation at Transonic and Supersonic Speeds of the Longitudinal Stability and Control Characteristics of an Airplane Configuration With a Thin Straight Wing of Aspect Ratio 3. NACA RM L9K25a, 1950.

12. Nelson, Robert L., and Stoney, William E., Jr.: Pressure Drag of Bodies at Mach Numbers up to 2.0. NACA RM L53I22c, 1953.

13. Patterson, R. T.: A Wind-Tunnel Investigation of the Drag of Conical Missile Afterbodies at Mach Numbers From 0.40 to 2.47 (TED No. TMB AD-3154). Aero. Rep. 857, David Taylor Model Basin, Navy Dept., Jan. 1954.

14. Van Driest, E. R.: Turbulent Boundary Layer in Compressible Fluids. Jour. Aero. Sci., vol. 18, no. 3, Mar. 1951, pp. 145-160, 216.

15. Welsh, Clement J., Wallskog, Harvey A., and Sandahl, Carl A.: Effects of Some Leading-Edge Modifications, Section and Plan-Form Variations, and Vertical Position on Low-Lift Wing Drag at Transonic and Supersonic Speeds. NACA RM L54K01, 1955.

16. Mitcham, Grady L., Crabill, Norman L., and Stevens, Joseph E.: Flight Determination of the Drag and Longitudinal Stability and Control Characteristics of a Rocket-Powered Model of a 60° Delta-Wing Airplane From Mach Numbers of 0.75 to 1.70. NACA RM L51I04, 1951.

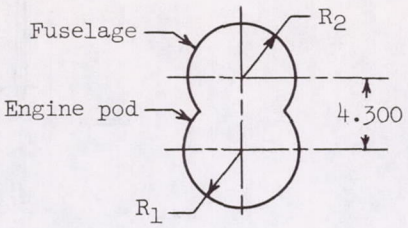
17. Henderson, Arthur, Jr.: Pitching-Moment Derivatives C_{M_q} and $C_{M_{\dot{\alpha}}}$ at Supersonic Speeds for a Slender-Delta-Wing and Slender-Body Combination and Approximate Solutions for Broad-Delta-Wing and Slender-Body Combinations. NACA TN 2553, 1951.

TABLE I

GEOMETRIC PARAMETERS OF CONFIGURATION

Fuselage and engine pod:	
Maximum frontal area, sq ft	0.340
Engine pod base area, sq ft	0.0925
Jet-exit area, sq ft	0.0786
Wing:	
Aspect ratio	2.31
Taper ratio	0
Mean aerodynamic chord, ft	1.711
Total plan form area, sq ft	3.80
Vertical fin:	
Aspect ratio (to fuselage center line)	0.895
Taper ratio (to fuselage center line)	0.514
Airfoil section	Hexagonal airfoil
Area (extended to fuselage center line) sq ft	0.804
Auxiliary fins (for one fin):	
Aspect ratio (to engine pod center line)	1.064
Taper ratio (to engine pod center line)	0.504
Airfoil section	Flat plate
Area (extended to engine pod center line)	0.709

TABLE II.- FUSELAGE ORDINATES



[Letter dimensions apply only to this table and all dimensions are given in inches]

Fuselage station	R_1	R_2
0	0	-----
1.000	.250	-----
2.000	.480	-----
3.000	.710	-----
5.000	1.130	-----
7.500	1.570	-----
10.000	1.955	-----
12.500	2.252	-----
15.000	2.429	-----
17.500	2.500	-----
22.625	2.500	0
23.015	2.500	.097
23.210	2.500	.145
23.600	2.500	.239
24.575	2.500	.469
26.525	2.500	.902
28.475	2.500	1.298
30.425	2.500	1.658
34.325	2.500	2.267
38.225	2.500	2.730
42.125	2.500	3.047
46.025	2.500	3.218
49.925	2.500	3.248
53.825	2.500	3.221
57.725	2.500	3.161
61.625	2.500	3.069
65.525	2.500	2.943
69.425	2.500	2.785
70.063	2.500	2.754
73.325	2.349	2.594
77.225	2.089	2.371
77.625	2.065	2.345
81.125	-----	2.115
85.025	-----	1.826
87.625	-----	1.615
89.925	-----	1.310
92.225	-----	.835
94.625	-----	0

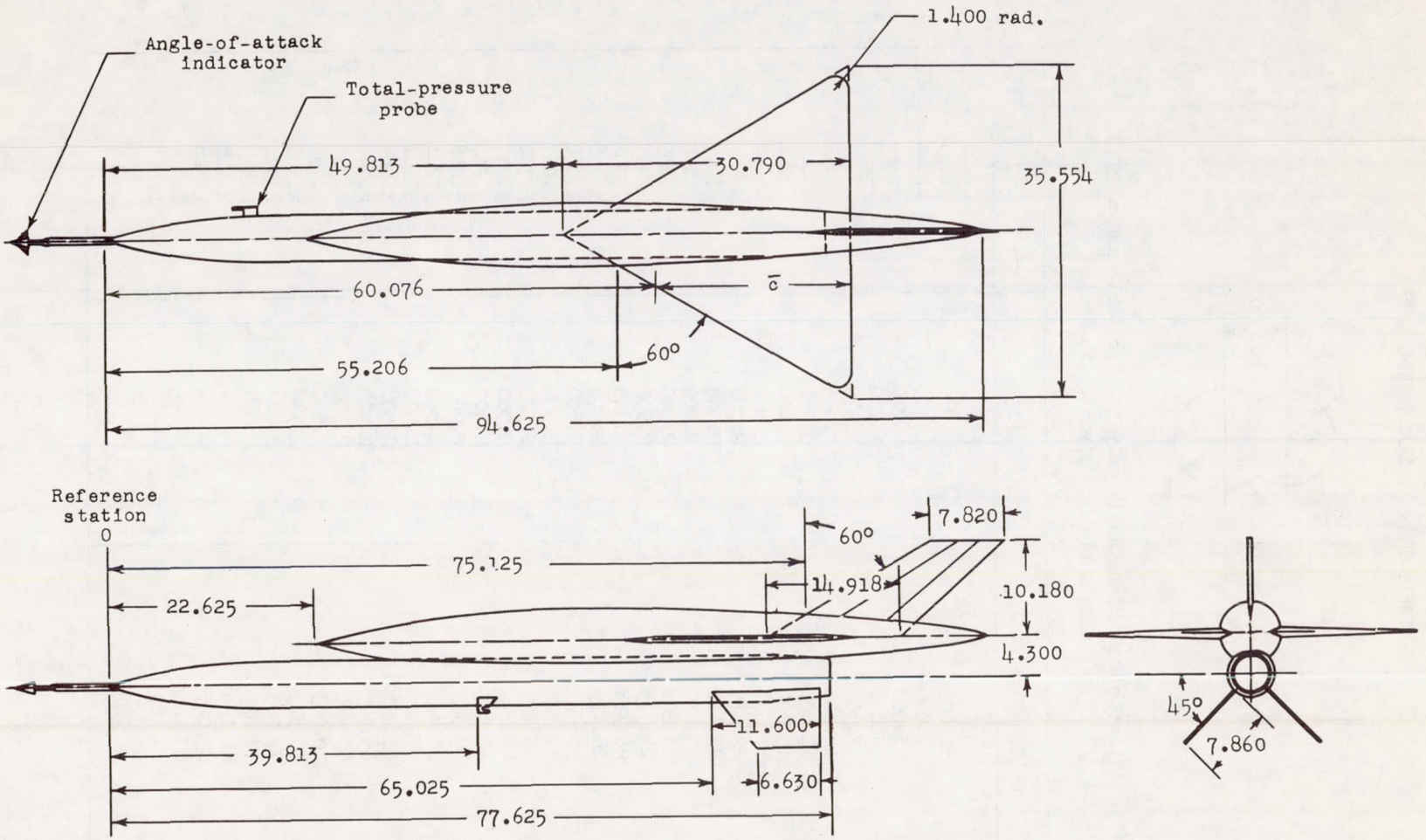


Figure 1.- Three-view drawing of the flight test model. All dimensions are in inches.

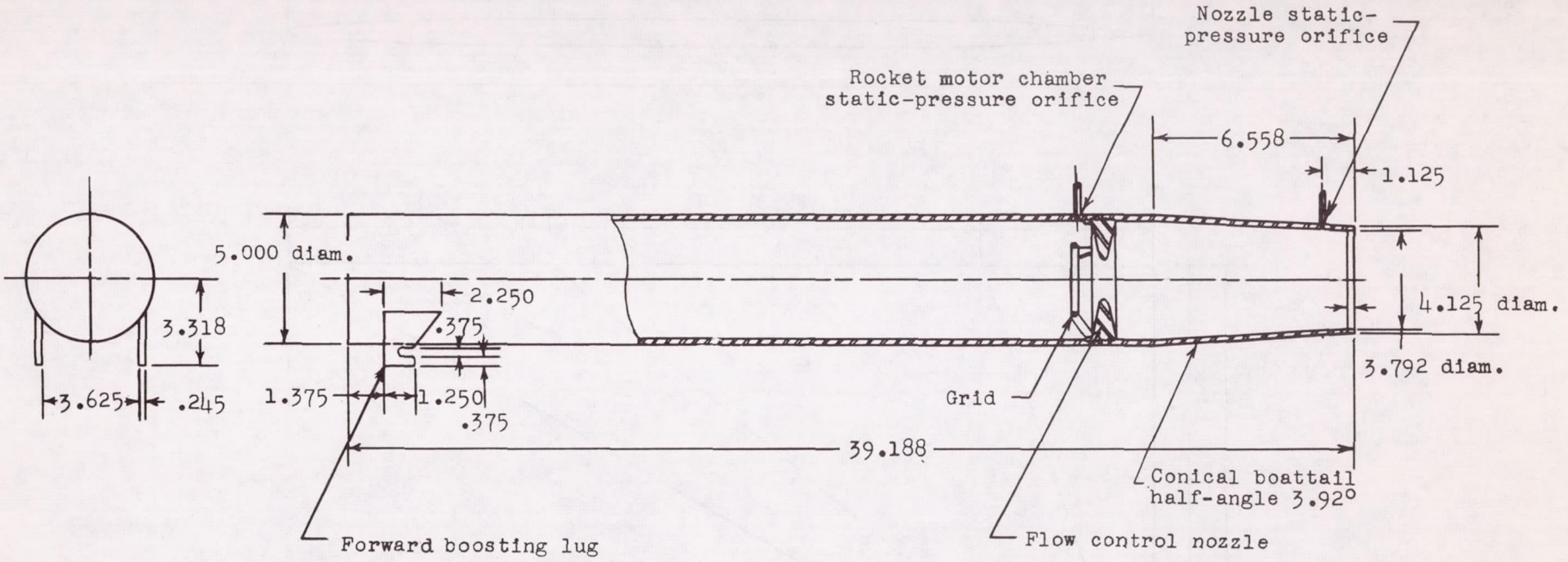


Figure 2.- Drawing of turbojet simulator. All dimensions are in inches.

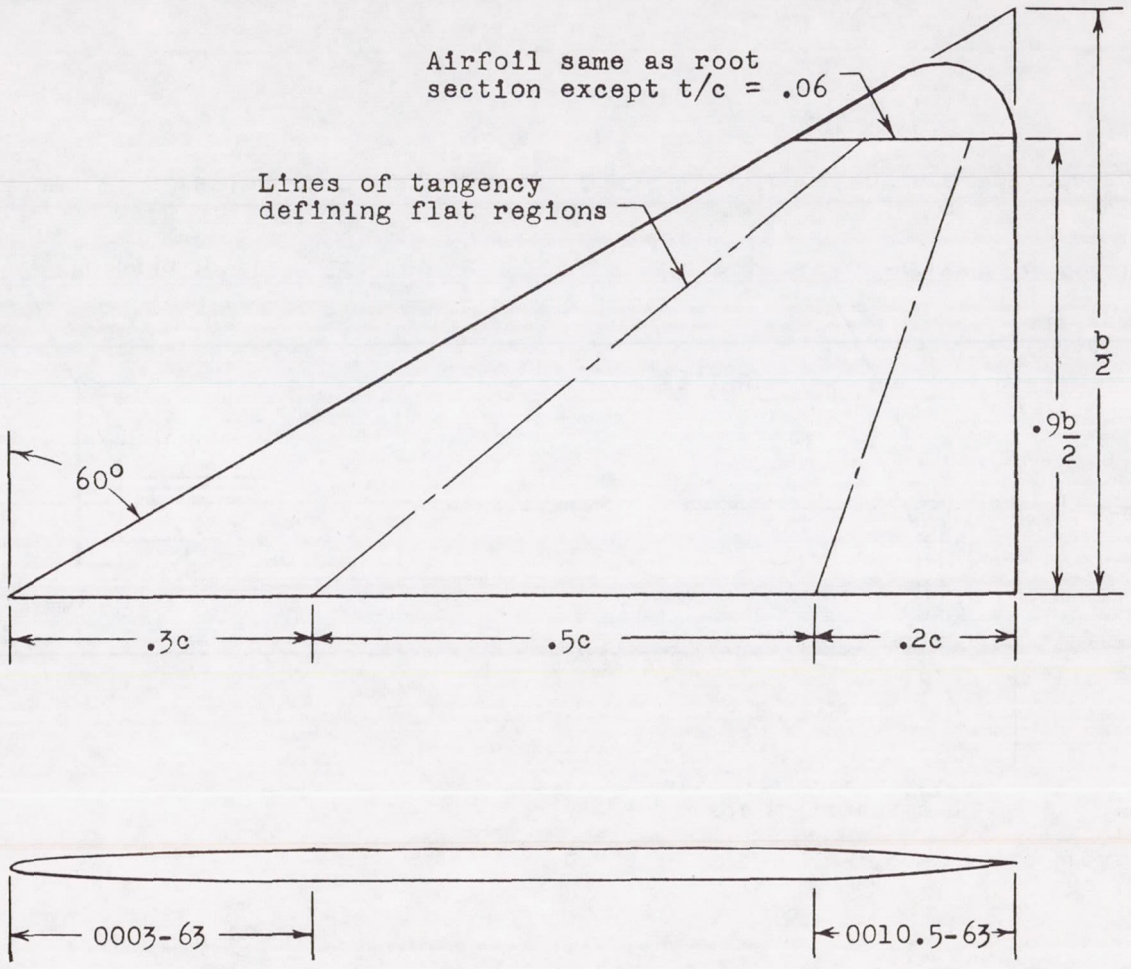
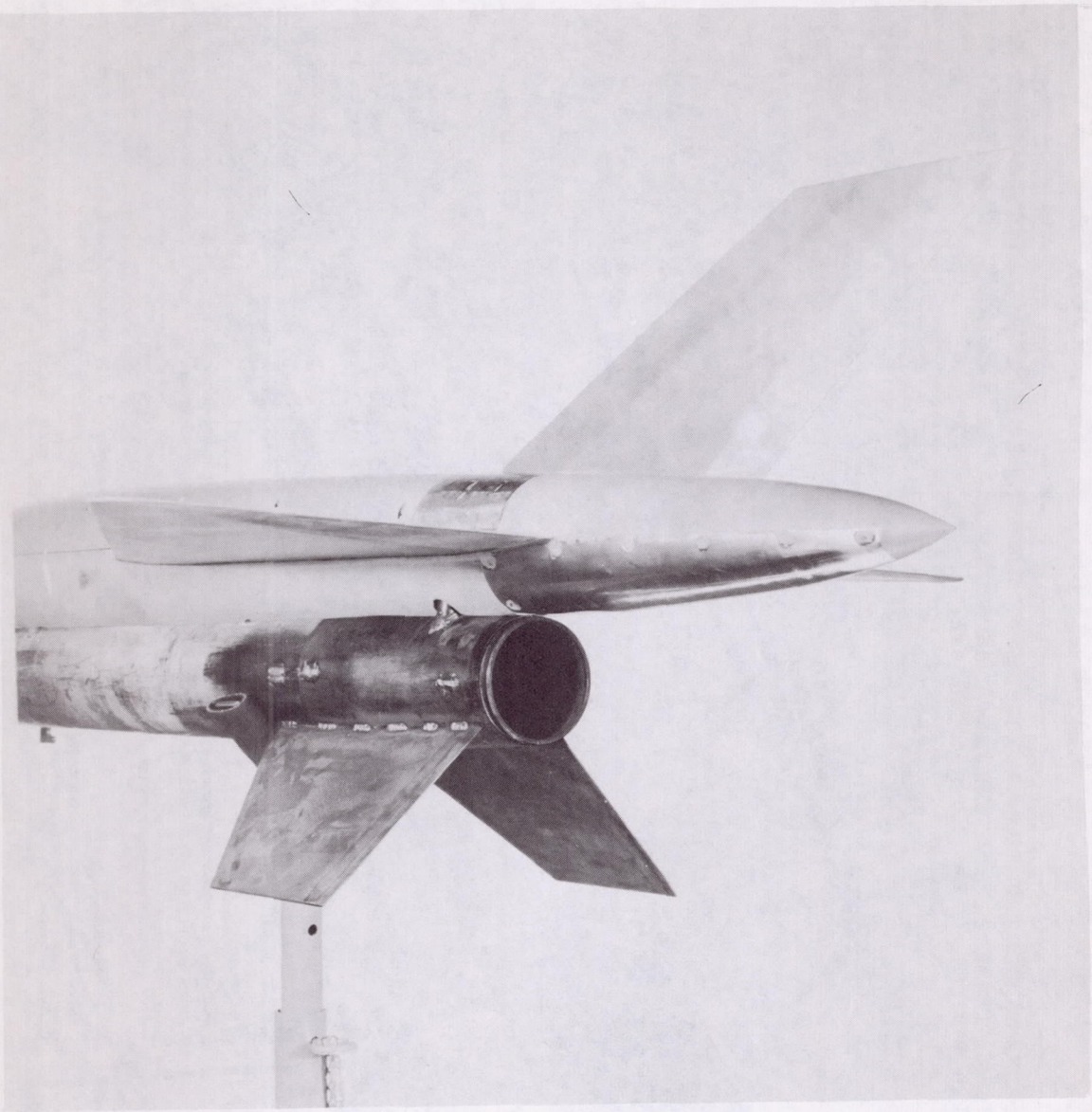
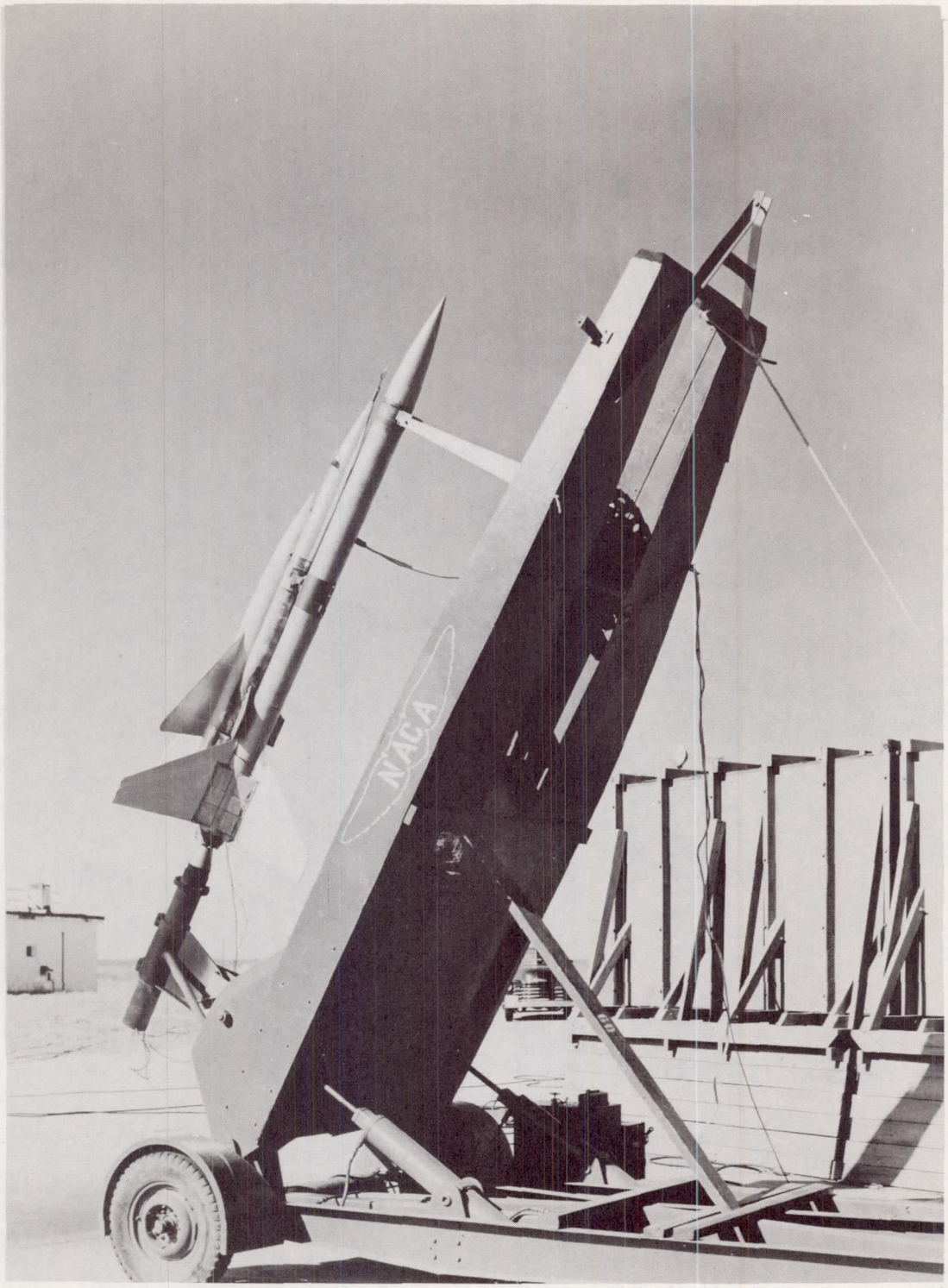


Figure 3.- Geometry of wing.



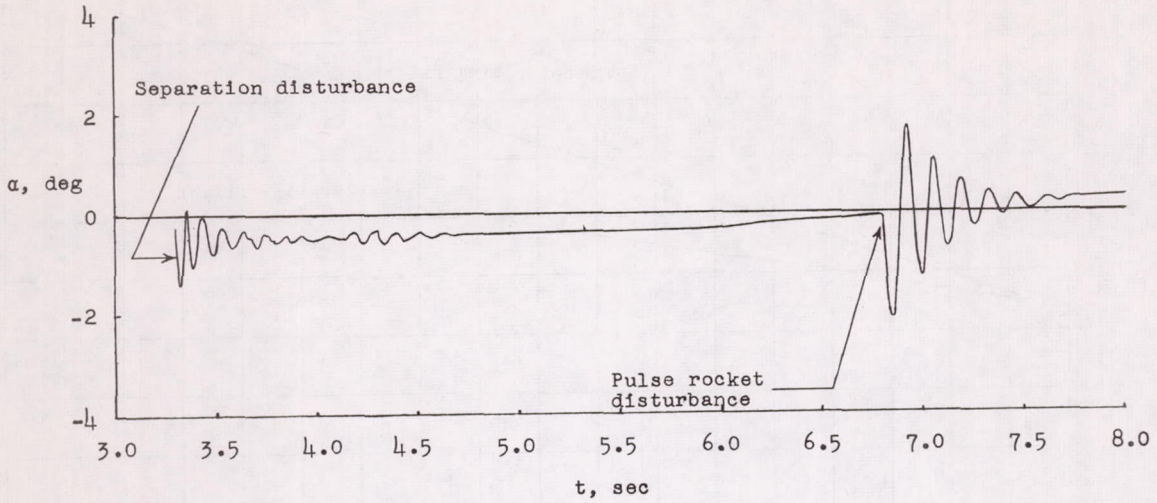
L-88340

Figure 4.- Photograph of tail section of flight model.

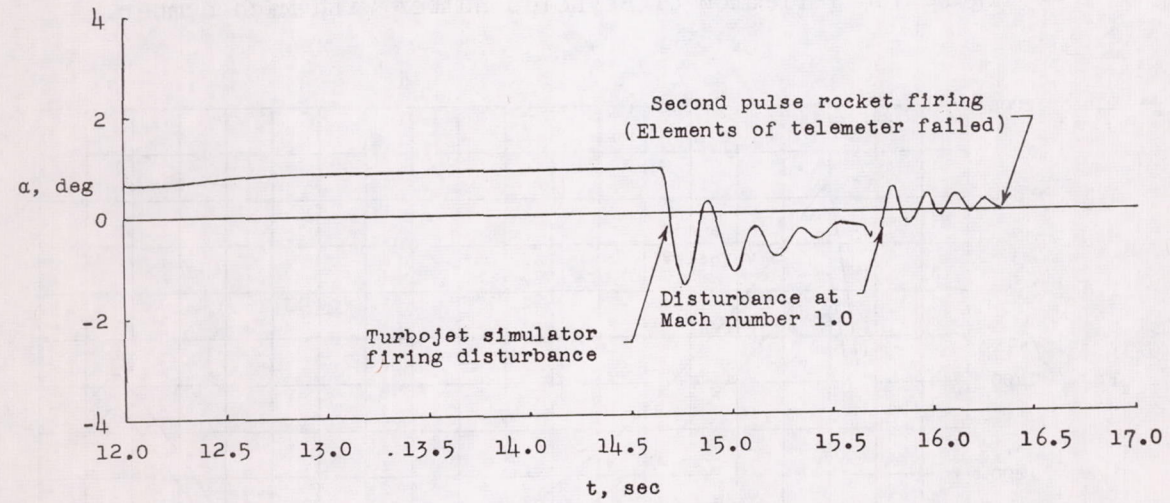


L-89053.1

Figure 5.- Model and booster on mobile launcher.



(a) Initial portion of decelerating flight.



(b) Latter portion of decelerating flight and initial portion of accelerating flight.

Figure 6.- Variation of angle of attack with time.

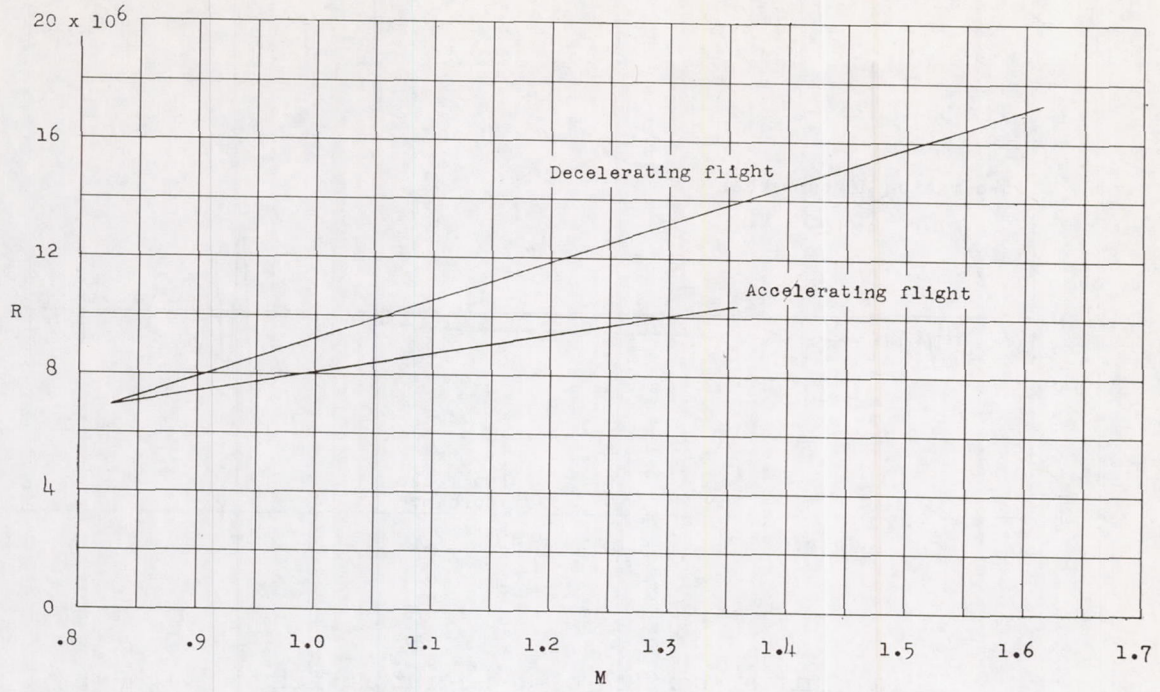


Figure 7.- Variation of Reynolds number with Mach number.

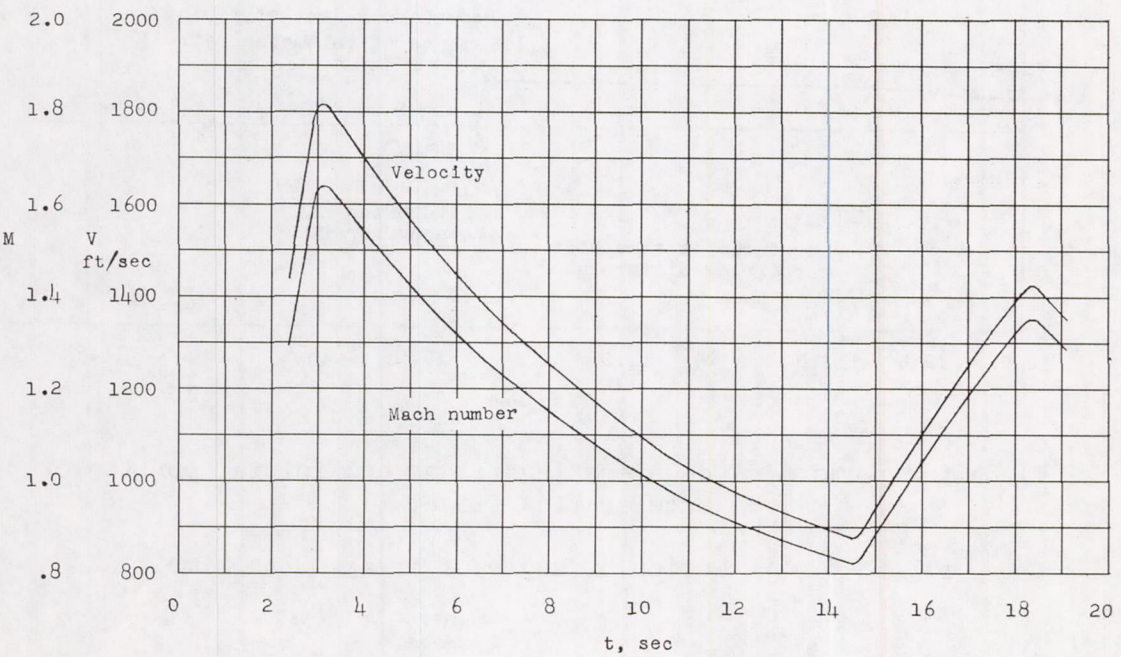


Figure 8.- Variation of model velocity and Mach number with time.

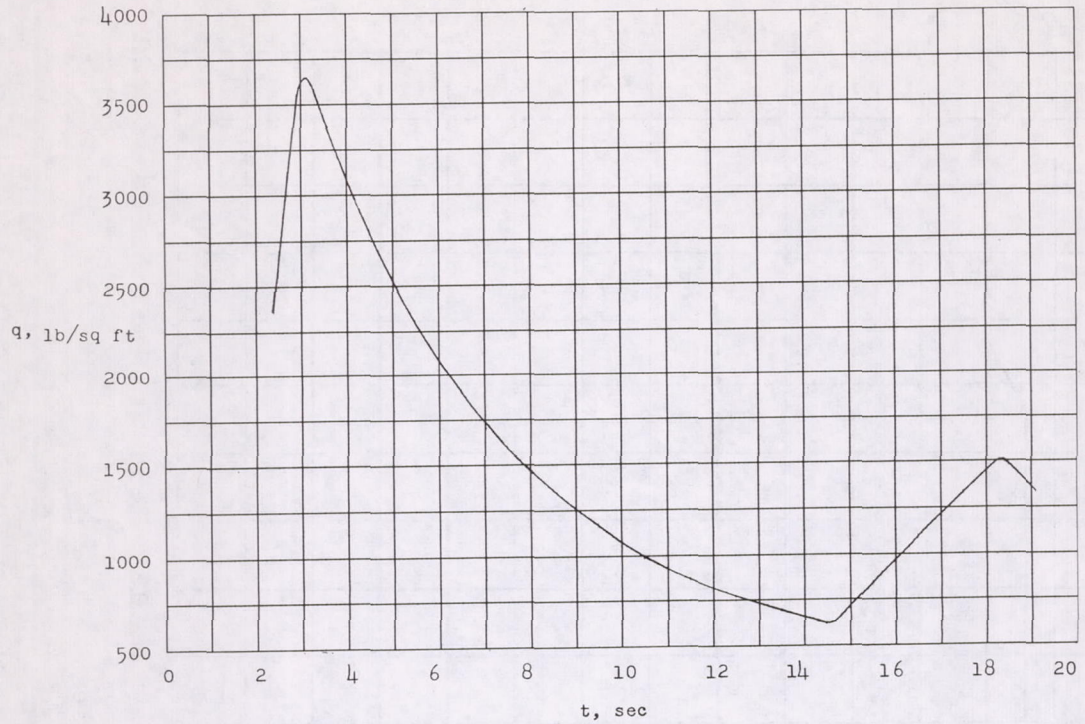


Figure 9.- Variation of dynamic pressure with time.

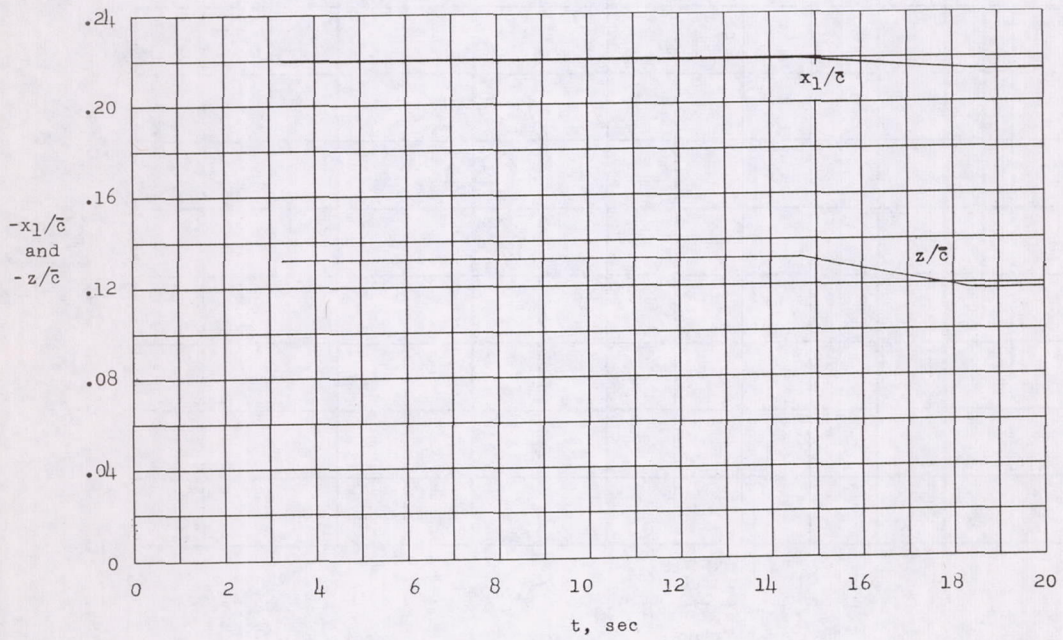


Figure 10.- The variation of center-of-gravity position, measured from the leading edge of the wing mean aerodynamic chord, with time.

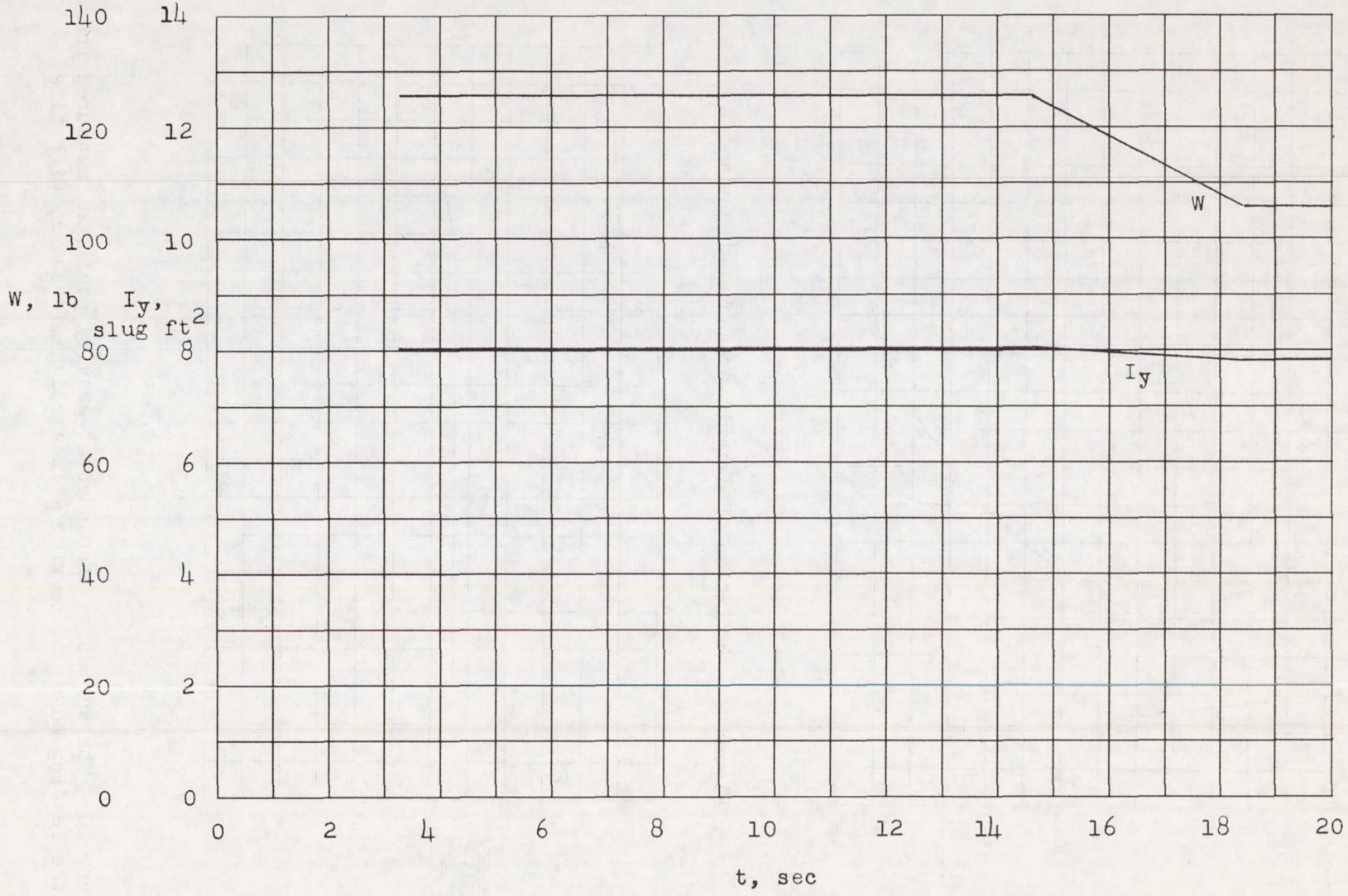
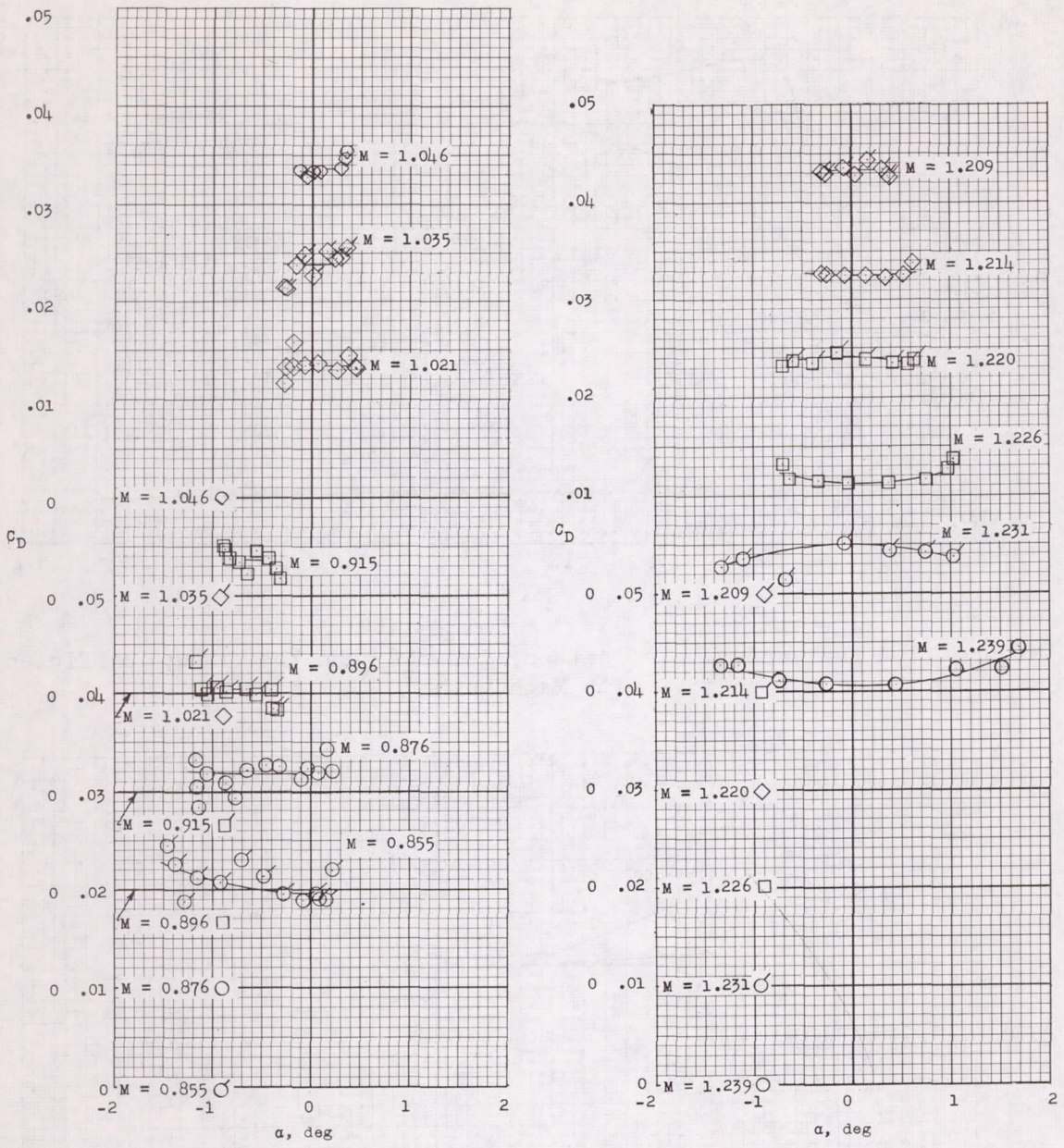


Figure 11.- The variation of model weight and moment of inertia with time.



(a) Jet-on drag coefficients. (b) Jet-off drag coefficients.

Figure 12.- The variation of drag coefficients with angle of attack obtained during pitching oscillations. Flagged symbols indicate increasing angle of attack; unflagged symbols indicate decreasing angle of attack.

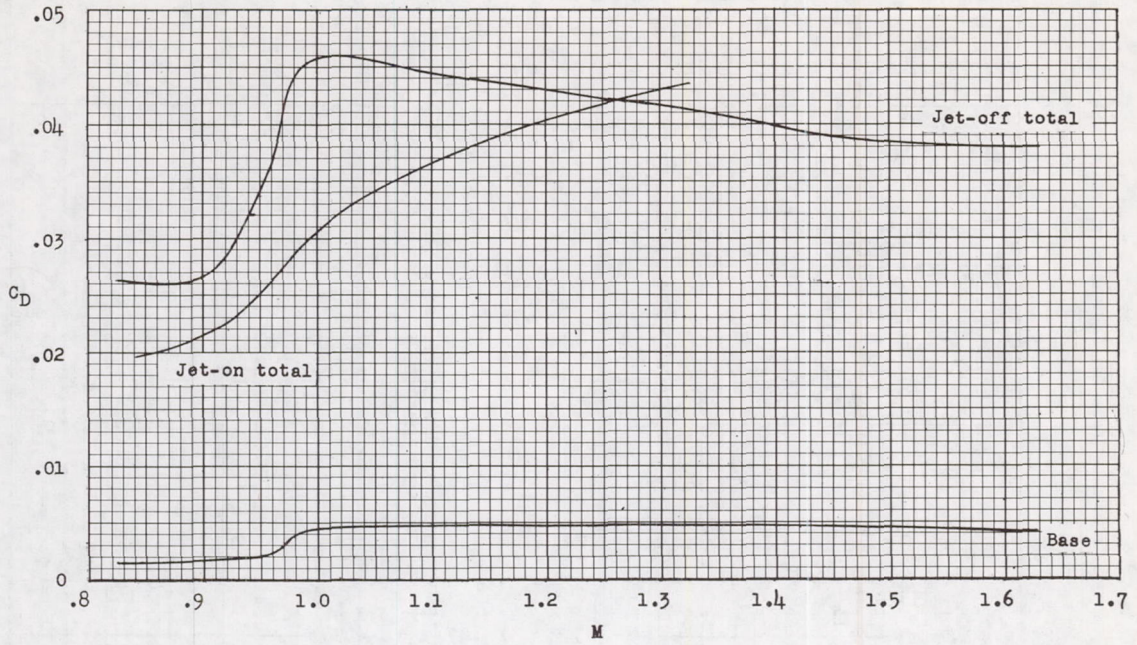


Figure 13.- The variation of jet-on, jet-off, and base drag coefficients with Mach number.

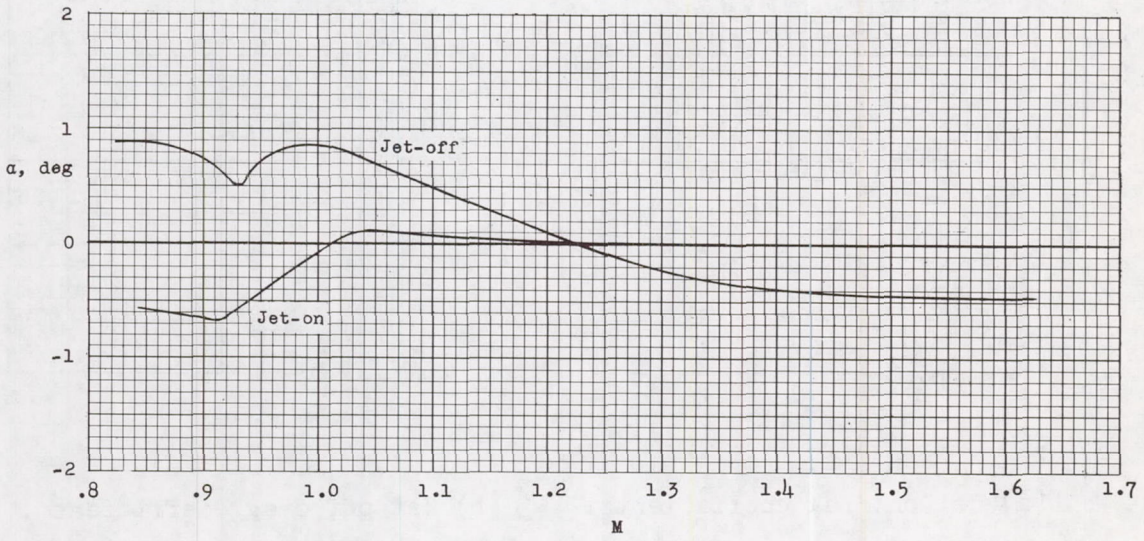


Figure 14.- The variation of trim angle of attack for jet-on and jet-off flight with Mach number.

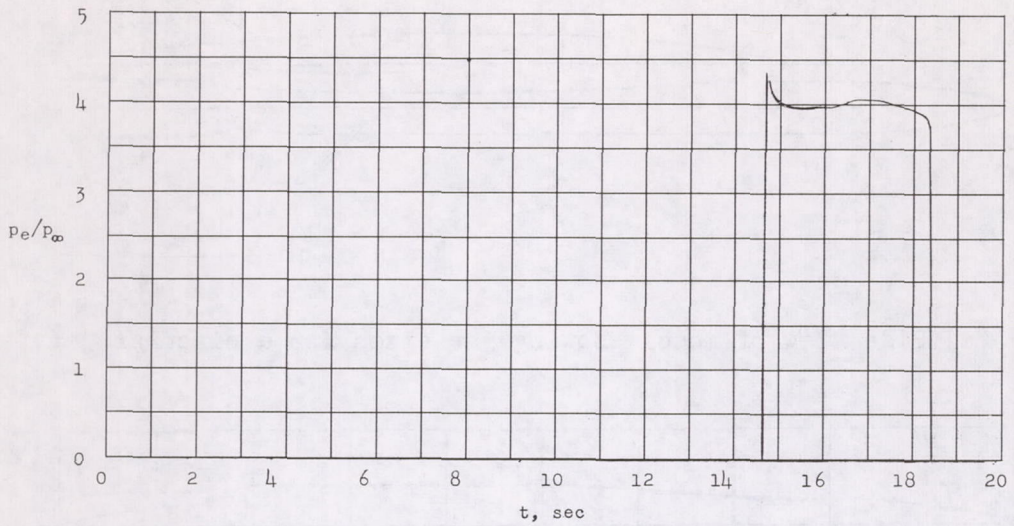


Figure 15.- The variation of jet static-pressure-ratio with time.

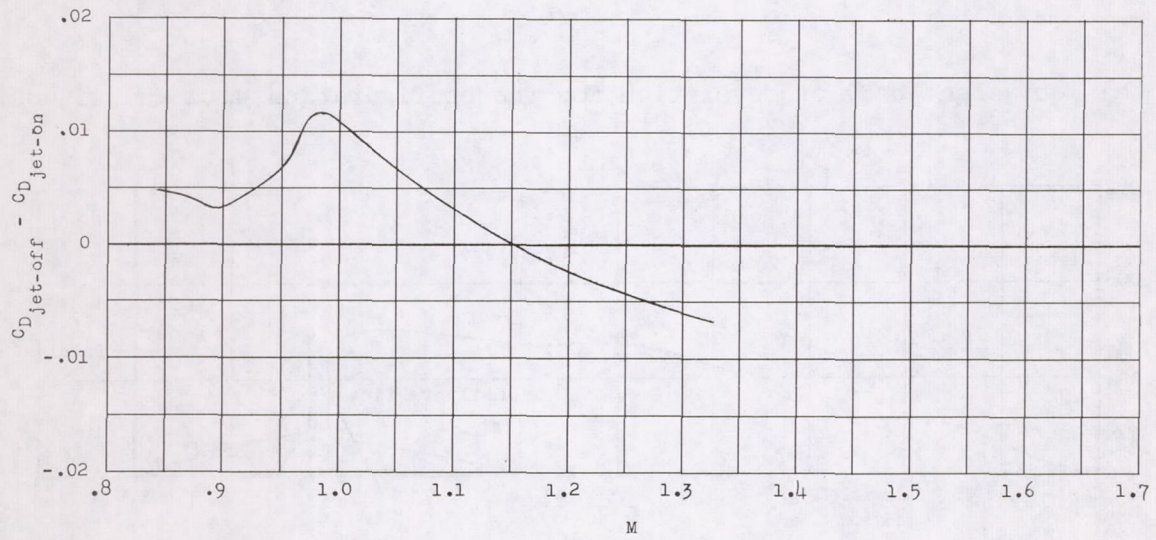
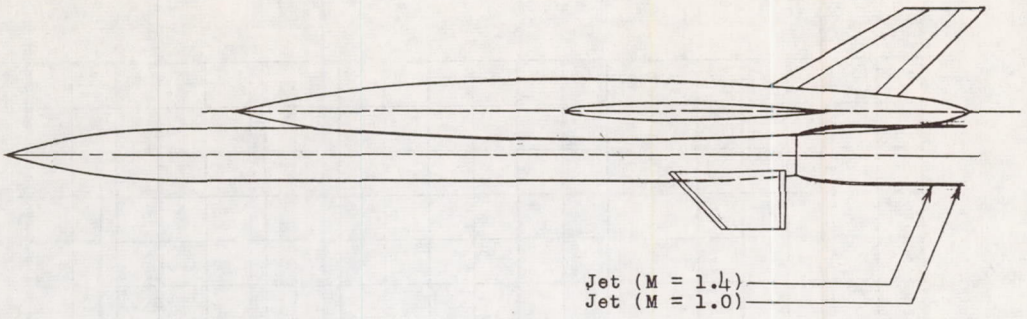
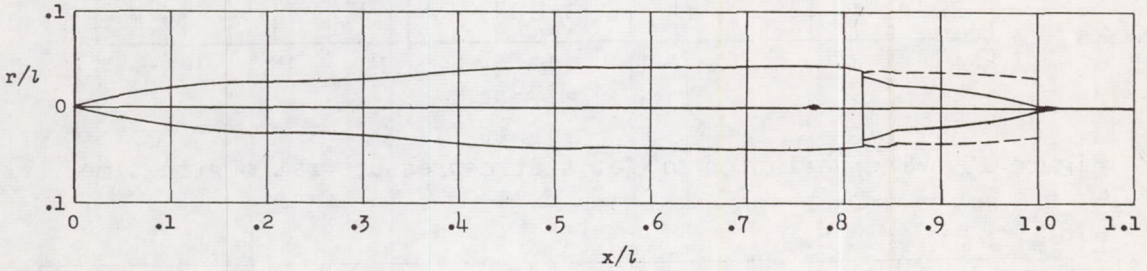


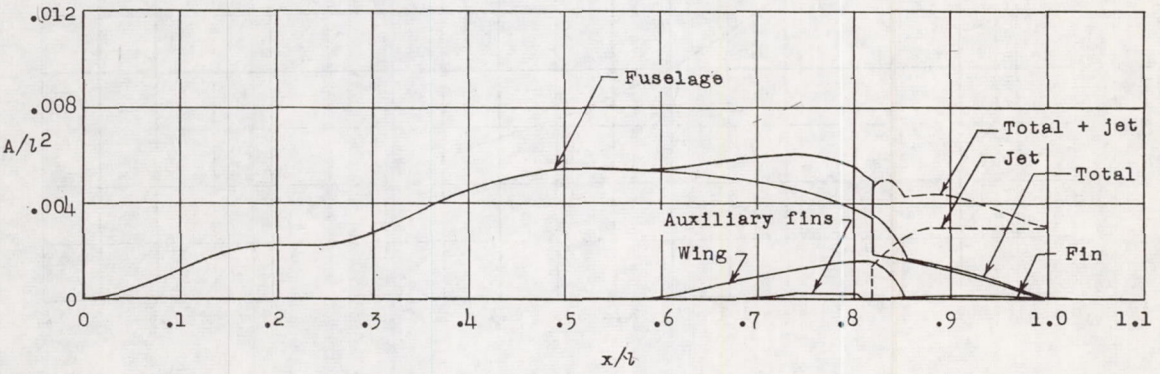
Figure 16.- The variation of the difference between jet-off and jet-on drag coefficients with Mach number.



(a) Side view of model showing jet sizes for a circular jet.



(b) Equivalent body of revolution for the configuration with and without the jet.



(c) Cross-sectional area distribution of the configuration with and without the jet.

Figure 17.- The effect of the jet on the cross-sectional area distribution of the configuration.

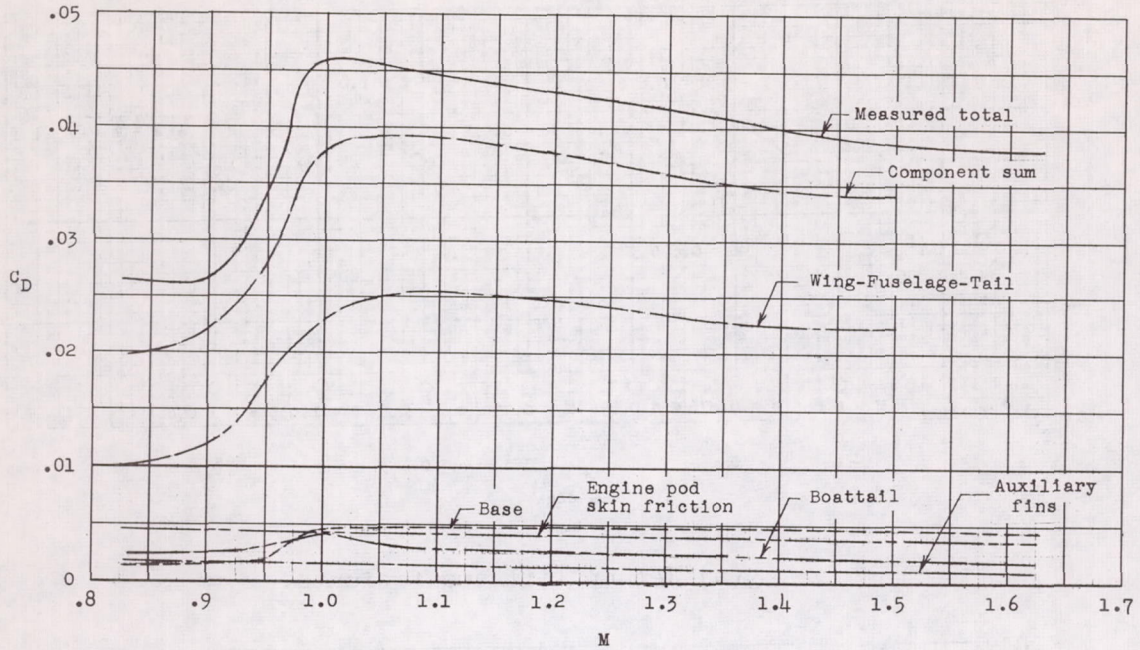


Figure 18.- The variation of the measured and estimated total-drag coefficients and the drag coefficients of the components with Mach number.

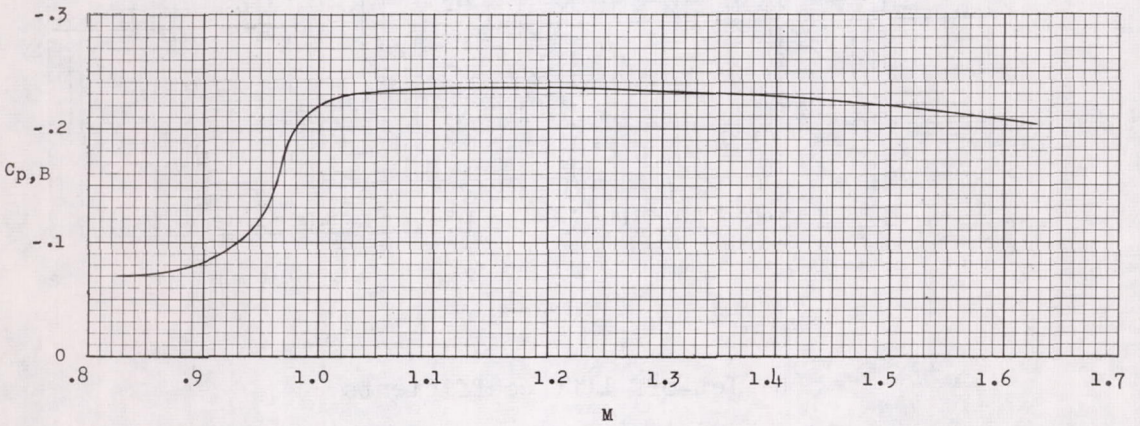
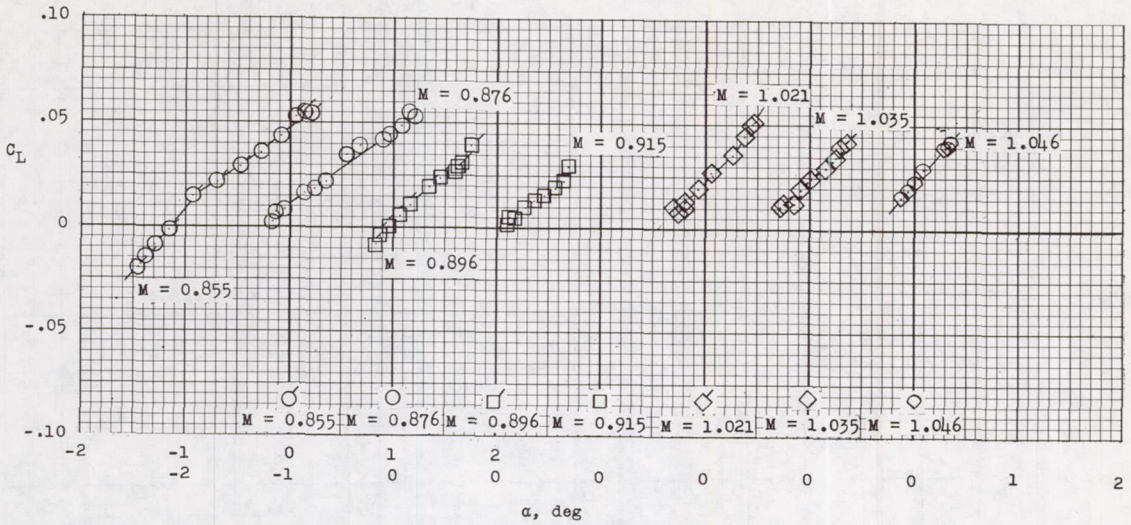
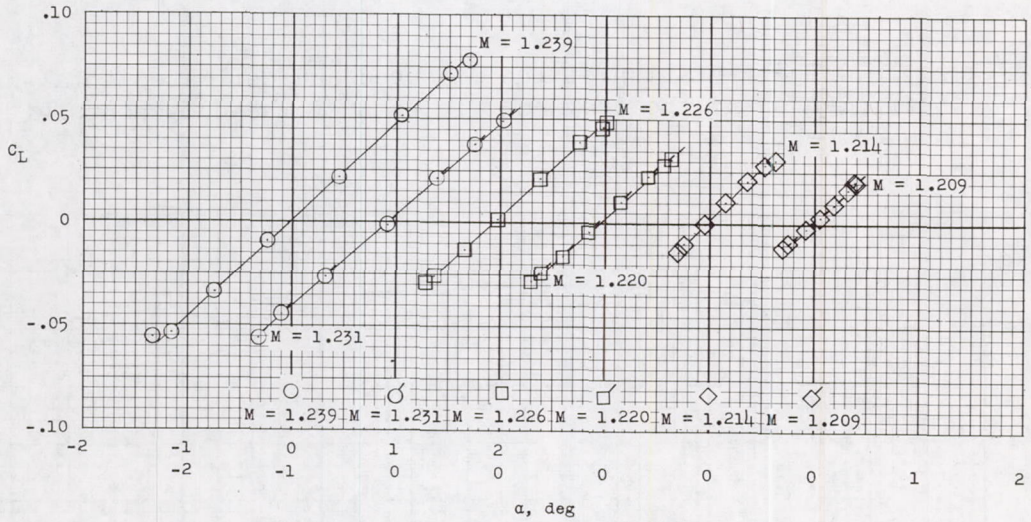


Figure 19.- The variation of the base pressure coefficient of the engine pod with Mach number.



(a) Jet-on lift coefficients.



(b) Jet-off lift coefficients.

Figure 20.- The variation of lift coefficients with angle of attack obtained during pitching oscillations. Flagged symbols indicate increasing angle of attack; unflagged symbols indicate decreasing angle of attack.

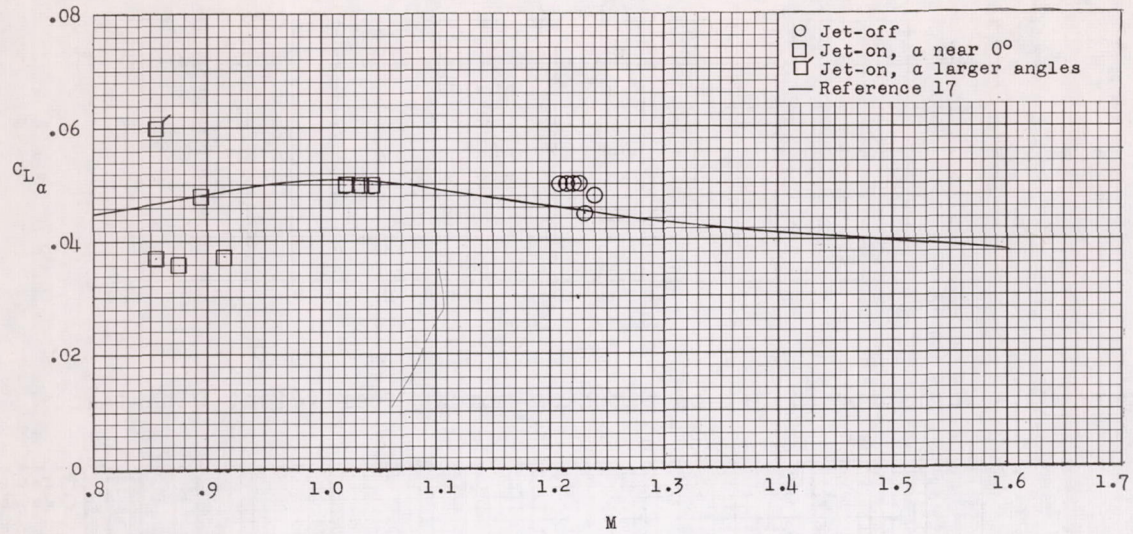


Figure 21.- The variation of lift-curve slope with Mach number.

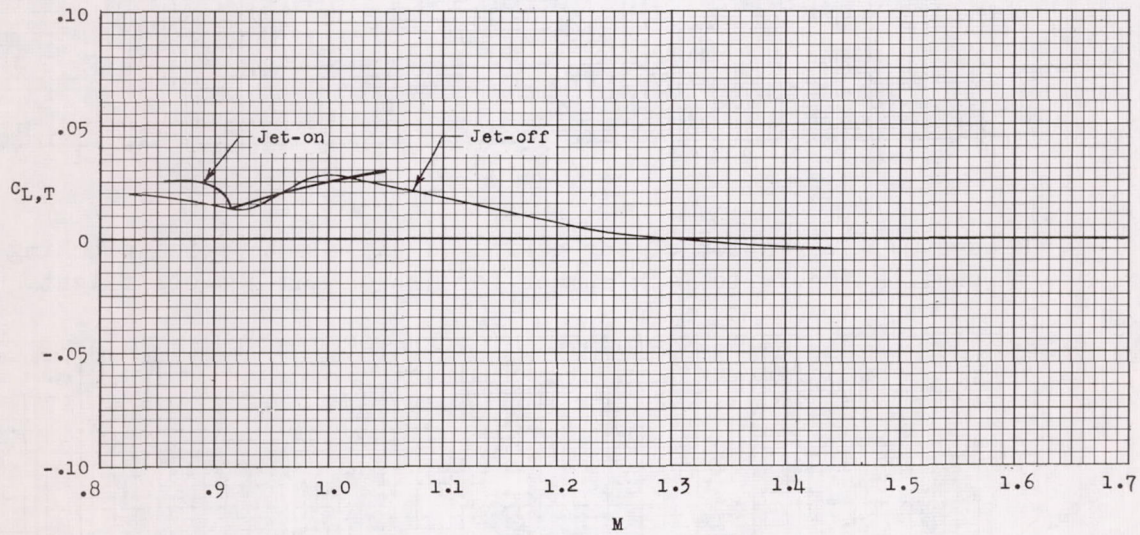


Figure 22.- The variation of trim-lift coefficient with Mach number.

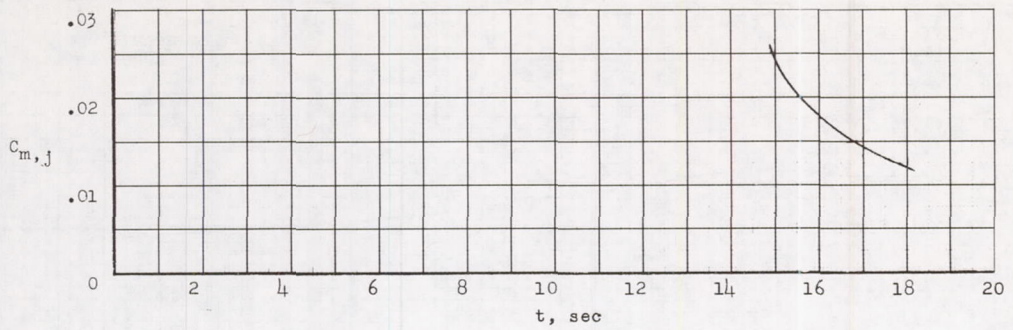


Figure 23.- Variation of jet-on pitching-moment coefficient with time.

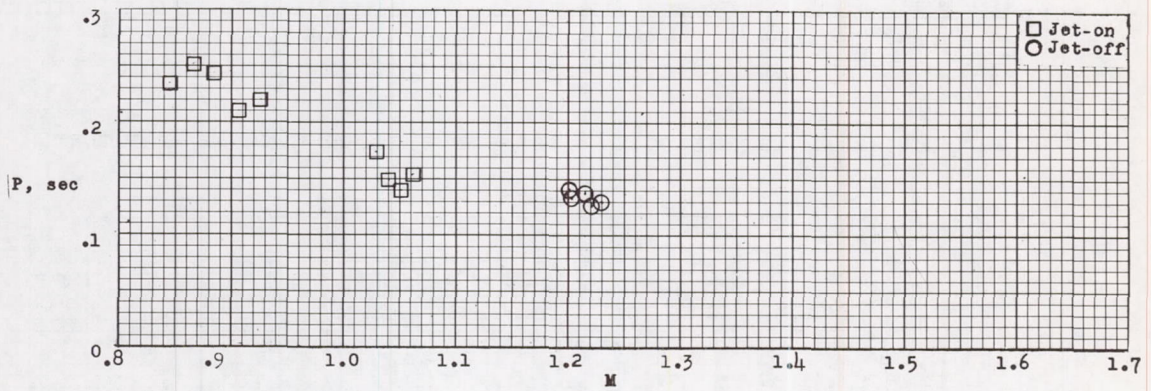


Figure 24.- Variation of the period of the short period pitching oscillations with Mach number for jet-on and jet-off flight.

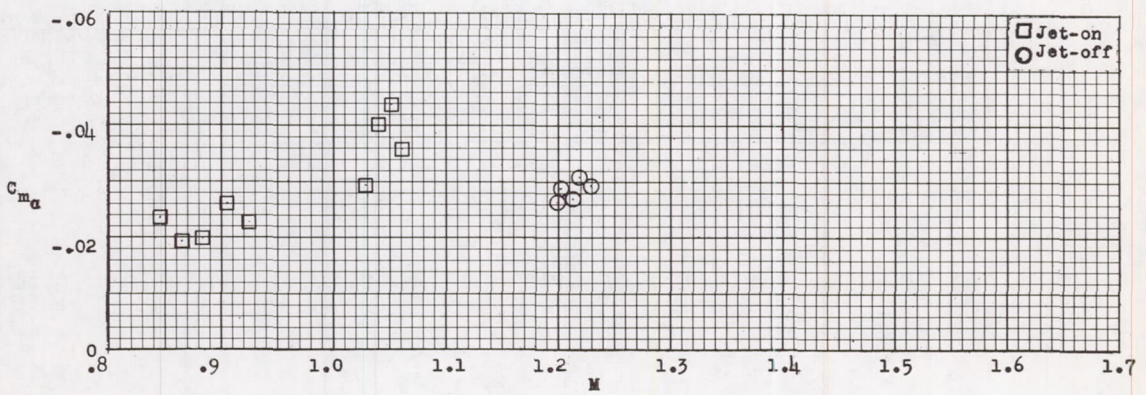


Figure 25.- Variation of static-stability derivative with Mach number for jet-on and jet-off flight.

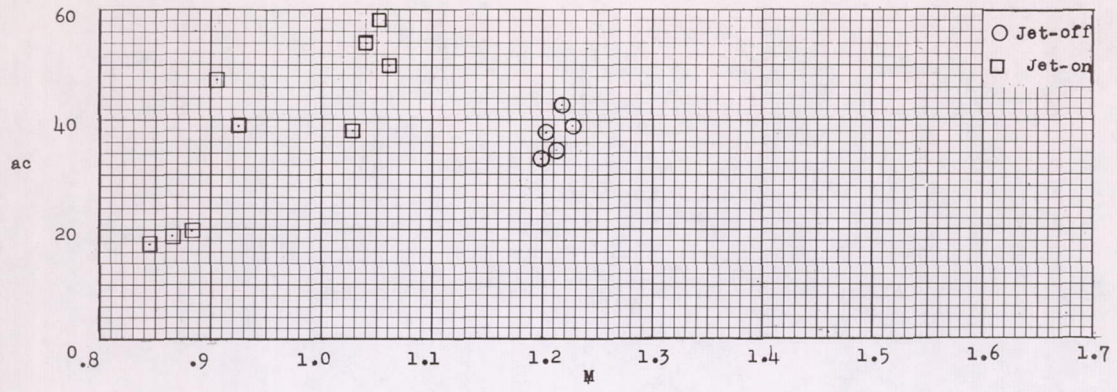


Figure 26.- Variation of aerodynamic center with Mach number for jet-on and jet-off flight.

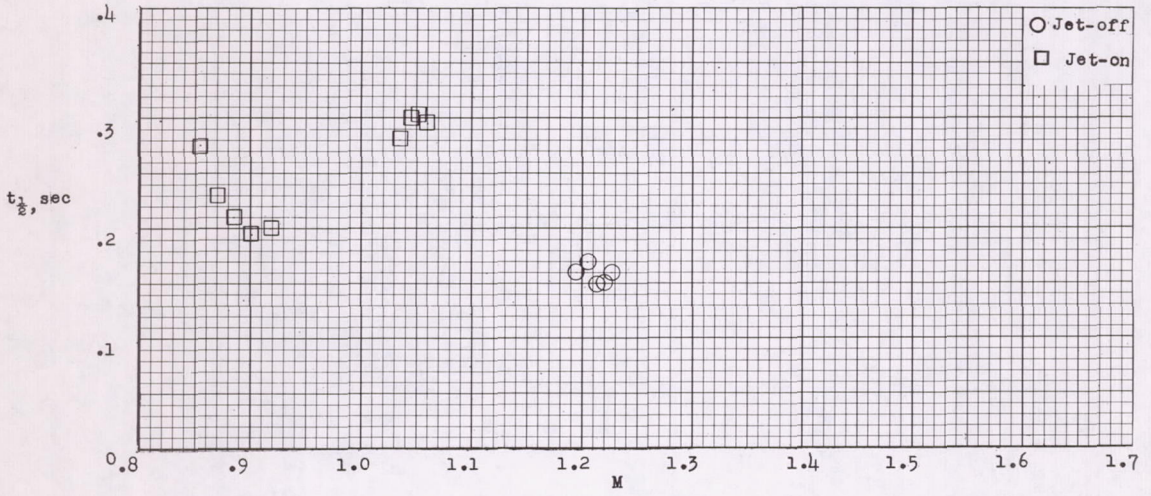


Figure 27.- Variation of the time to damp to one-half amplitude with Mach number for jet-on and jet-off flight.

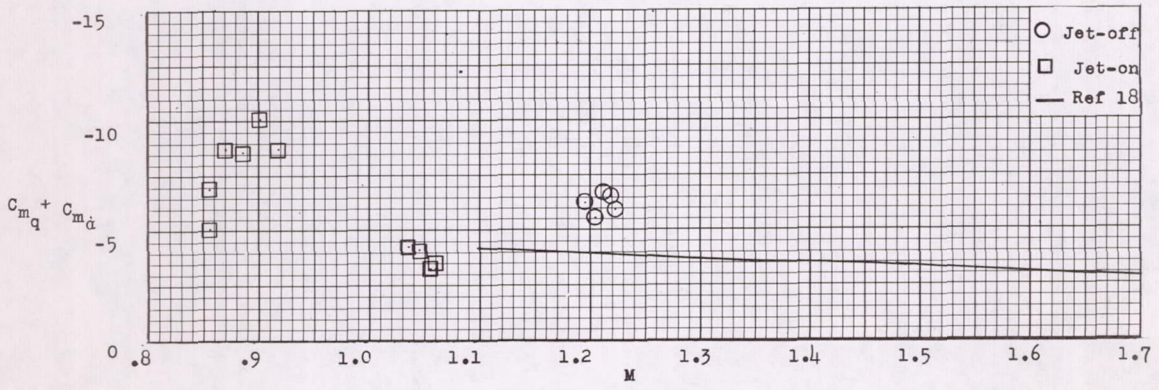


Figure 28.- Variation of damping derivatives with Mach number for jet-on and jet-off flight.